

05,07

Magnetostructural phenomena in hydrides of metastable Laves phases $RMn_2D_{3-\delta}$

© O.L. Makarova¹, I.N. Goncharenko², A.V. Tsvyashchenko³, L.N. Fomicheva³

¹ National Research Center „Kurchatov Institute“,
Moscow, Russia

² Leon Brillouin Laboratory, CEA,
Saclay, France

³ Vereshchagin Institute of High Pressure Physics of the Russian Academy of Sciences,
Troitsk, Moscow, Russia

E-mail: cukalfa@mail.ru

Received November 15, 2023

Revised December 15, 2023

Accepted January 18, 2023

We have studied the processes of atomic and magnetic ordering in the hydrides of the metastable Laves phases $RMn_2D_{3-\delta}$ ($R = Y, Tb, \text{ and } Dy; \delta \leq 0.14$) in the temperature range from 2 to 300 K and the pressure range from 0 to 6 GPa by X-ray and neutron diffraction methods. We found that a hydrogen superstructure with symmetry reduction to $P6_3/m$ is formed in the hydrides $RMn_2D_{3-\delta}$ near room temperature. A number of unusual magnetic phenomena that have never been observed in the hexagonal Laves hydrides RMn_2D_x was found, namely, the coexistence of ferrimagnetic and antiferromagnetic orderings in $RMn_2D_{3-\delta}$ ($R = Tb, Dy$) and pressure-induced transition from the ferrimagnetic to antiferromagnetic state in $TbMn_2D_{2.86}$. It has been suggested that the topology of the crystal lattice plays an important role in the formation of the magnetic properties of the hexagonal hydrides $RMn_2D_{3-\delta}$.

Keywords: rare earth intermetallics, hydrides, magnetostructural transition, neutron diffraction, high pressures.

DOI: 10.61011/PSS.2024.02.57917.255

1. Introduction

Interest in intermetallic compounds based on rare earth and transition metals is due, among other things, to their unique magnetic properties. These compounds readily absorb hydrogen and form stable hydrides. In a number of cases, treatment in a hydrogen atmosphere improves their magnetic characteristics [1,2]. In addition to the applied aspect, hydrides of intermetallic compounds are convenient model objects for studying the physical properties of materials with the aim of their controlled change. Thus, in the compounds RMn_2D_x (R — rare earth metal) it was experimentally discovered that hydrogen ordering induces magnetic order in the manganese sublattice [3,4], and in the paper [5] it was suggested that it is possible to control hydrogen ordering in RFe_2D_x using a magnetic field. In both cases the topology of the crystal and magnetic sublattices plays a decisive role. Depending on the type of rare earth atom, compounds RMn_2 crystallize in cubic (C15) or hexagonal (C14) structural types, at that both cubic and hexagonal hydrides RMn_2D_x show a close relationship between magnetic and hydrogen ordering. In cubic hydrides $RMn_2D_{4.2}$ ($R = Y, Gd, Tb, Dy, Ho$) the magnetostructural transitions are observed, at them the hydrogen and magnetic sublattices are ordered simultaneously [3,4]. In hexagonal hydrides RMn_2D_x ($R = Er, Tm, Lu$) states with short- and long-range magnetic order alternate as the hydrogen content

increases [6,7]. Synthesis at high pressures and temperatures makes it possible to obtain a metastable hexagonal modification of compounds RMn_2 [8], which have cubic symmetry under ordinary conditions, which makes it possible to directly study the role of crystal structure topology in the formation of magnetic and hydrogen subsystems. In this paper, the processes of hydrogen and magnetic ordering in hydrides of metastable Laves phases $RMn_2D_{3-\delta}$ ($R = Y, Tb \text{ and } Dy; \delta \leq 0.14$) in the temperature range from 2 to 300 K and pressures of 0 to 6 GPa were studied by neutron and X-ray diffraction method. The main parameters of the crystalline and magnetic structures are determined.

2. Experiment procedure

The initial samples RMn_2 were produced by electric arc melting from Mn (99.99%) and rare earth metals Y, Tb, Dy (99.9%). To obtain a hexagonal modification, they were subjected to heat treatment at a temperature above 1500 °C and a pressure of 8 GPa in toroid-type chambers at Vereshchagin Institute of High Pressure Physics [9]. The crystalline structure and phase analysis of the obtained samples were refined by X-ray diffraction at 300 K. In addition to the hexagonal modification RMn_2 , traces of the phases R_2O_3 and R_6Mn_{23} were observed in X-ray patterns, their number did not exceed 5%. The hydrides were synthesized at the Scientifica Research Center „Kurchatov

Institute“ by direct saturation with hydrogen from the gas phase, at that using the heavy isotope deuterium in to reduce incoherent scattering in neutron experiments. Neutron diffraction measurements were carried out on G6.1 diffractometer installed at the Orpheus reactor (Saclay, France) in the temperature range from 2 to 280 K. To study the structure at high pressures, G6.1 diffractometer was used in a configuration specially adapted for studying small-volume samples in high-pressure chambers [10]. Neutron diffraction patterns were processed by full-profile Rietveld analysis using program FullProf [11].

3. Results

X-ray diffraction studies carried out at 300 K showed that the arrangement of metal atoms in the initial compounds RMn_2 , synthesized at high pressure, and their hydrides $RMn_2D_{3-\delta}$ ($R = Y, Tb, Dy$; $\delta \leq 0.14$) corresponds to the structure type C14. In hexagonal hydrides $RMn_2D_{3-\delta}$ increase in the volume per one interstitial hydrogen atom, of so-called. „hydrogen volume“ exceeds the values observed in their cubic analogues.

Neutron diffraction spectra of hydrides $RMn_2D_{3-\delta}$, measured in the temperature range of 2 to 280 K and processed by the Rietveld method, are shown in Figure. 1. Over the entire temperature range the crystalline structure retains hexagonal symmetry. In the diffraction patterns of hydrides measured near room temperature, a peak (1 1 1) is observed, it is forbidden in the space group $P6_3/mmc$, which supposes that in these compounds hydrogen is ordered and, possibly, this state is maintained up to the temperature of hydrogen desorption. Experimental spectra measured near room temperature were compared with models of equiprobable distribution of hydrogen atoms over interstitial sites of certain types (R_2Mn_2 , RMn_3 , Mn_4). The best agreement with experiment was obtained for the model in which hydrogen atoms are distributed among the interstitial sites R_2Mn_2 . In the lattice cell of the hydride RMn_2D_3 containing 4 formula units, 12 hydrogen atoms are distributed among 48 interstitial sites R_2Mn_2 . The number of options for the hydrogen atoms distribution in the sublattice interstitial sites can be reduced if we take into account the decrease in the symmetry of the crystal, which is indicated by the superstructural peak (1 1 1) and the blocking of neighboring interstitial sites by introduced hydrogen within a radius of 2.2 Å [12]. A model, in which the symmetry of the crystal is reduced to $P6_3/m$ and 12 hydrogen atoms are distributed among 18 interstitial sites R_2Mn_2 , satisfying the blocking conditions, gives the best agreement with experiment for all hydrides. During the diffraction spectra processing the lattice periods, parameters of crystallographic positions, and the coefficients of crystallographic positions occupation with hydrogen were refined at fixed values of the isotropic factors of thermal displacement of atoms. Crystalline structure parameters obtained from X-ray and neutron diffraction data near room temperature are given in Table 1.

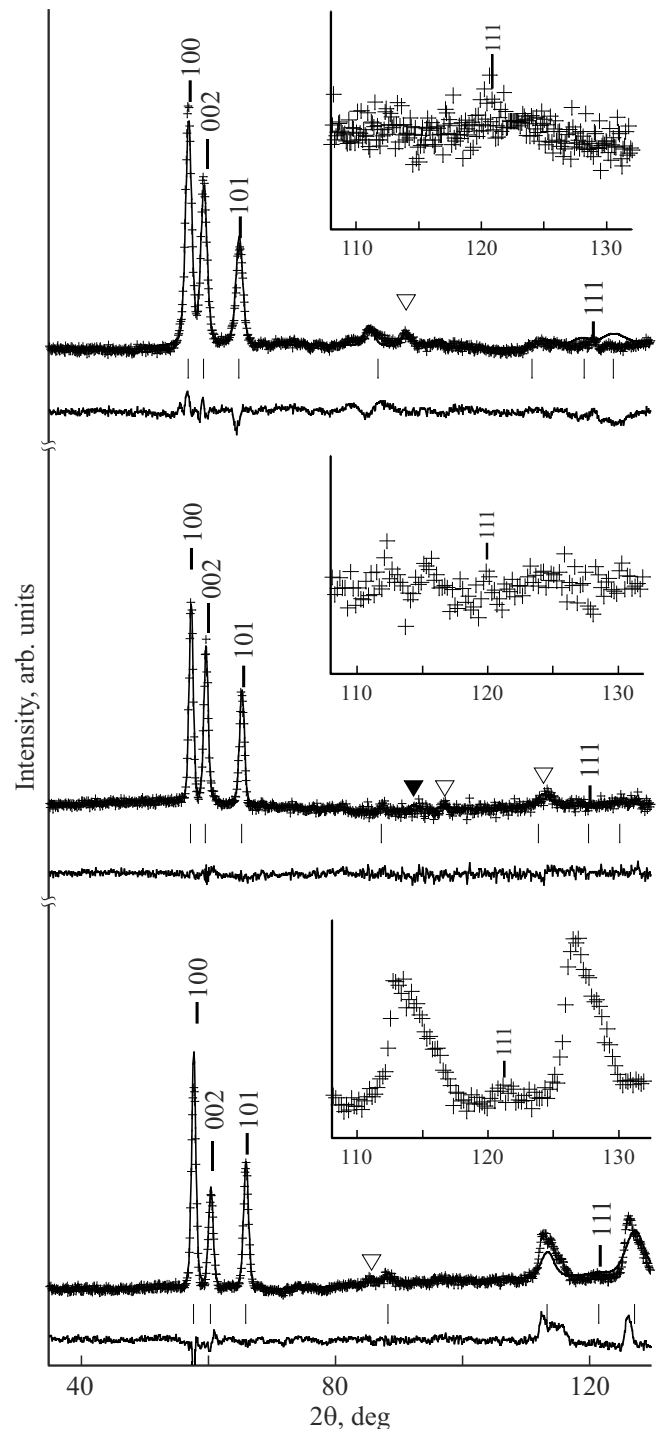


Figure 1. Neutron diffraction spectra of hydrides $RMn_2D_{3-\delta}$ (top to bottom YMn_2D_3 , $TbMn_2D_{2.86}$ and $DyMn_2D_{2.89}$). The experimental points obtained at temperature of 280 K, as well as the profile, difference curve and peak positions calculated using the model given in Table 1 are shown. Traces of NaCl and RD_3 impurities in the spectrum are marked by filled and unfilled triangles, respectively. The inserts show a fragment of the diffraction spectrum containing the superstructural peak (1 1 1). The scale of the vertical axis on the inserts is increased by 10 times.

Table 1. Crystalline structure parameters of hydrides $RMn_2D_{3-\delta}$ ($R = Y, Tb$ and Dy), obtained from X-ray and neutron diffraction spectra at temperature of 280 K. Space group $P6_3/m$. The values of the lattice periods (a, c), the volume of the primitive cell (V), the volume per one introduced hydrogen atom (V_D), the ratio of the axes (c/a), positional parameters (x, y, z) of crystallographic positions and the probability of their occupation by atoms (p) were determined, as well as matching factors R_p, R_{wp} . The values of the thermal factors are fixed, for R atoms they were 0.2 \AA^2 , for Mn atoms — 0.4 \AA^2 , for D atoms — 1.3^2 \AA^2 [7]

Parameters	$Y Mn_2 D_3$	$Tb Mn_2 D_{2.86}$	$Dy Mn_2 D_{2.89}$
$a, \text{ \AA}$	5.7249(2)	5.6823(2)	5.6759(1)
$c, \text{ \AA}$	9.4993(6)	9.4748(5)	9.4255(3)
$V, \text{ \AA}^3$	67.4(2)	66.2(2)	65.7(1)
$V_D, \text{ \AA}^3$	4.03	4.20	4.12
c/a	1.6593	1.6674	1.6606
$R 4f (\frac{1}{3}, \frac{2}{3}, z) z$	0.0638(6)	0.0640(7)	0.0626(6)
$Mn 6h (x, y, \frac{1}{4}) x$	-0.1728(13)	-0.1676(21)	-0.1697(49)
y	-0.3456(26)	-0.3352(42)	-0.3394(98)
$D 12i (x, y, z) x$	0.0435	0.0435	0.0435
y	0.3259	0.3259	0.3259
z	0.5406(25)	0.5310(36)	0.5433(70)
p	0.609(4)	0.617(6)	0.510(10)
$D 6h (x, y, \frac{1}{4}) x$	0.4920(7)	0.4782(20)	0.4861(10)
y	0.9839(14)	0.9563(40)	0.9721(20)
p	0.782(4)	0.672(7)	0.888(10)
$R_p, \%$	10.7	5.83	14.5
$R_{wp}, \%$	11.0	6.10	12.5

In the diffraction patterns of all hydrides, measured below 200 K, significant changes in the intensity distribution were observed. It was found that the increase in the intensity of additional scattering tends to decrease as the scattering angle increases; and the temperature, at which additional scattering occurs, corresponds to the temperature of magnetic ordering in hexagonal hydrides RMn_2D_3 ($R = Er, Tm, Lu$) [7]. Besides, in hydrides $RMn_2D_{3-\delta}$ ($R = Tb, Dy$) changes in the intensity of structural lines turn out to be so large that they can not be explained by hydrogen atoms redistribution. The listed features allowed us to assume the magnetic origin of the additional scattering. Figure 2 shows the magnetic contribution to the diffraction spectra of hydrides $RMn_2D_{3-\delta}$, obtained by subtracting the spectra measured in the paramagnetic region. The intensities of the structural lines in the diffraction patterns of hydride $Y Mn_2 D_3$ change slightly in the temperature range of 280 to 180 K; with further cooling down to the lowest temperatures, the structural lines do not change. Below 180 K in the diffraction patterns a weak additional scattering is observed, it can be characterized by the wave vector $[1/3 1/3 0]$. The temperature, at which additional scattering occurs, and the value of the wave vector correspond to the parameters of the antiferromagnetic order previously

discovered in $Lu Mn_2 D_x$ systems [6,7]. In the diffraction patterns of the hydrides $Tb Mn_2 D_{2.86}$ and $Dy Mn_2 D_{2.89}$ the intensities of the structural lines do not change upon cooling from 280 to 200 K. Below 200 K the increase in the intensity of structure lines is observed, as well as additional

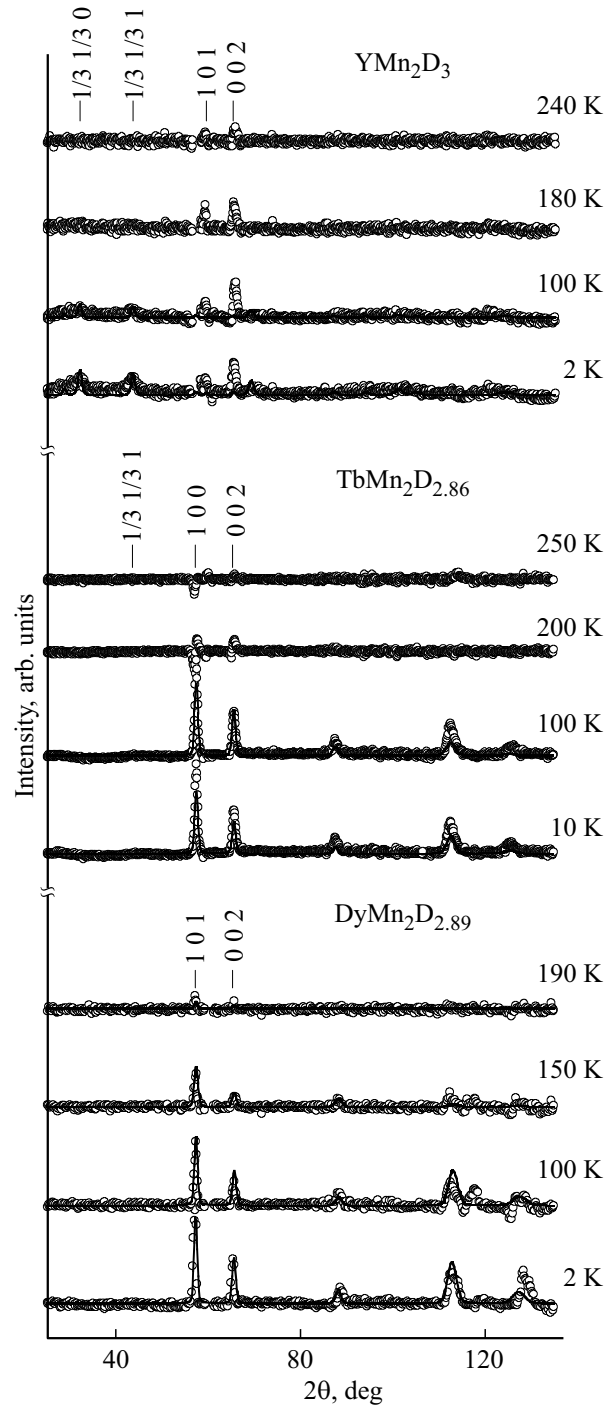


Figure 2. Magnetic contribution to the neutron diffraction spectra of $Y Mn_2 D_3$, $Tb Mn_2 D_{2.86}$ and $Dy Mn_2 D_{2.89}$. Spectra measured at various temperatures are presented, from which spectra measured in the paramagnetic region are selected. The experimental points and profiles calculated based on the model presented in Tables 2 and 3 are shown.

diffuse scattering, which can be described by the wave vector $[1/3\ 1/3\ 0]$. The observed features allow us to assume that at temperatures below 200 K the antiferromagnetic order is formed in YMn_2D_3 , and in $\text{DyMn}_2\text{D}_{2.86}$ and $\text{TbMn}_2\text{D}_{2.89}$ the complex magnetic state is realized, in which, along with the ferromagnetic component, there is antiferromagnetic component.

During the processing of diffraction spectra measured below the magnetic transition temperature, additionally to the structural parameters the magnitudes and directions of the magnetic moments were refined. For the hydride YMn_2D_3 the calculations were carried out in magnetic sublattice basis that was increased by three times compared to the chemical sublattice basis. Independent variation in the magnitude and direction of the magnetic moments for each atom made the procedure of successive iterations of the calculated spectrum unstable. To achieve satisfactory convergence of experimental and calculated data, the direction of the magnetic moments varied within the plane ab . For hydrides $\text{TbMn}_2\text{D}_{2.86}$ and $\text{DyMn}_2\text{D}_{2.89}$ the absence of magnetic contribution to the integral intensity of peak (002) clearly indicated that the magnetization vectors of R - and Mn -sublattices are oriented along the hexagonal axis c . The parameters of the magnetic structure obtained from diffraction data at temperature of 2 K are given in Table 2, 3. Note that the obtained values of the magnetic moments on atoms R and Mn are noticeably smaller than the values of the magnetic moments of free ions R^{3+} and the effective moment of the paramagnetic ion Mn^{3+} . The assumption that the decrease in the magnitude of magnetic moments is due to the formation of noncollinear magnetic structure did not find sufficient confirmation when processing experimental data. The position of superstructural lines found in $\text{TbMn}_2\text{D}_{2.86}$ and $\text{DyMn}_2\text{D}_{2.89}$, their blurriness

Table 2. Parameters of the magnetic structure YMn_2D_3 measured at a temperature of 2 K. The positional parameters of atoms (x, y, z) , projections of the magnetic moment onto the crystallographic axes M_x and M_y are given. Parameter M_z is equal to $0\ \mu_B$

Atom	Position	M_x, μ_B	M_y, μ_B
Mn_{11}	(0, 0, 0)	–	–
Mn_{12}	(0, 0, $\frac{1}{2}$)	–	–
Mn_{21}	($x, y, \frac{1}{4}$)	1.6 (0.4)	0
Mn_{22}	($-y, x - y, \frac{1}{4}$)	0	1.6 (0.4)
Mn_{23}	($-x + y, -x, \frac{1}{4}$)	-1.6 (0.4)	-1.6 (0.4)
Mn_{24}	($-x, -y, \frac{3}{4}$)	-1.6 (0.4)	0
Mn_{25}	($y, -x + y, \frac{3}{4}$)	0	-1.6 (0.4)
Mn_{26}	($x - y, x, \frac{3}{4}$)	1.6 (0.4)	1.6 (0.4)
$R_m, \%$		21%	

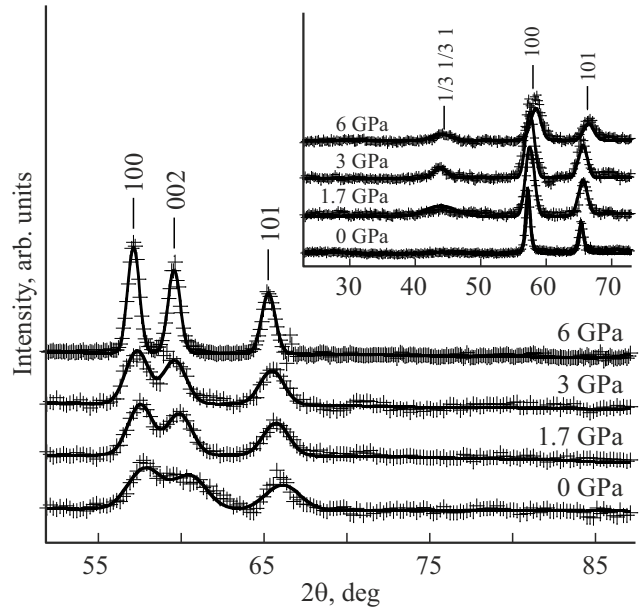


Figure 3. Neutron diffraction spectra of $\text{TbMn}_2\text{D}_{2.86}$ measured in the pressure range of 0 to 6 GPa and temperatures of 2 to 280 K. Experimental points, calculated spectra, and positions of structural peaks are presented. The insert shows spectra measured in the pressure range of 0 to 6 GPa at temperature of 2 K, from which spectra measured in the paramagnetic region are selected.

compared to well-formed magnetic scattering, arising in the positions of nuclear peaks, the appearance of these peaks at lower temperatures indicate that in hydrides with magnetic R -sublattice, in addition to ferrimagnetic ordering, there are correlations of short-range antiferromagnetic order.

Experiments at high pressures identified additional aspects of the magnetic order formation in hydride $\text{TbMn}_2\text{D}_{2.86}$. Figure 3 shows neutron diffraction spectra measured at temperature of 280 K and pressures up to 6 GPa in $\text{TbMn}_2\text{D}_{2.86}$. In the pressure range of 0 to 3 GPa, the crystalline structure retains hexagonal symmetry; a full-profile analysis of diffraction patterns was carried out using the crystalline structure model proposed in Table 1. The insert to Figure 3 shows the magnetic scattering spectra obtained by subtracting spectra measured in the paramagnetic region from low-temperature spectra for various pressures. According to experimental data, the hydride $\text{TbMn}_2\text{D}_{2.86}$ retains the ferrimagnetic structure in the pressure range of 0 to 3 GPa. The temperature of magnetic ordering and the magnitude of magnetization of R - and Mn -sublattices do not depend on the magnitude of the applied pressure. At pressures of 3 GPa and higher along with scattering, which can be characterized as a contribution from the ferrimagnetic phase, the well-formed superstructural peaks appear in the spectra, they are described by the wave vector $[1/3\ 1/3\ 0]$. The analysis of the temperature dependences of the intensities of superstructural peaks showed that they occur upon cooling below 150 K. When the sample is unloaded to

Table 3. Parameters of magnetic structure of hydrides $RMn_2D_{3-\delta}$ ($R = Tb$ and Dy) measured at temperature 2 K (11 K for $TbMn_2D_{2.86}$). The positional parameters of atoms (x, y, z), projections of the magnetic moment onto the crystallographic axis z M_z are given. Parameters M_x and M_y are equal to $0\mu_B$. Calculations were carried out on the basis of two models of the magnetic structure: in model 1 the values of the magnetic moments on the atoms Mn1 and Mn2 varied independently of each other, and in model 2 they were related

Atom	Position	$TbMn_2D_{2.86}$		$DyMn_2D_{2.89}$	
		Model 1	Model 2	Model 1	Model 2
		M_z, μ_B	M_z, μ_B	M_z, μ_B	M_z, μ_B
R_{1-4}	$(\frac{1}{3}, \frac{2}{3}, z), (\frac{2}{3}, \frac{1}{3}, z + \frac{1}{2}), (\frac{2}{3}, \frac{1}{3}, -z), (\frac{1}{3}, \frac{2}{3}, -z + \frac{1}{2})$	6.0 (0.1)	6.0 (0.1)	5.9 (0.2)	6.3 (0.2)
Mn_{1-2}	$(0, 0, 0), (0, 0, \frac{1}{2})$	3.0 (0.1)	-2.4 (0.1)	-1.2 (0.3)	-0.9 (0.3)
$Mn_{2_{1-6}}$	$(x, y, \frac{1}{4}), (-y, x - y, \frac{1}{4}), (-x + y, -x, \frac{1}{4}), (-x, -y, \frac{3}{4}),$ $(y, -x + y, \frac{3}{4}), (x - y, x, \frac{3}{4})$	2.1 (0.1)	-2.4 (0.1)	-0.4 (0.3)	-0.9 (0.3)
Rm, %		8.4	4.1	18.4	12.2

Table 4. Coordination environment of hydrogen atoms in hydrides $RMn_2H_{3-\delta}$. For tetragonal interstitial sites R_2Mn_2 the values of interatomic distances d_{D-Me} , interstitial site radii R , probabilities of interstitial sites occupation with hydrogen atoms p are given

Atom	YMn_2D_3			$TbMn_2D_{2.86}$			$DyMn_2D_{2.89}$		
	$d_{D-Me}, \text{Å}$	$R, \text{Å}$	p	$d_{D-Me}, \text{Å}$	$R, \text{Å}$	p	$d_{D-Me}, \text{Å}$	$R, \text{Å}$	p
D12i ₁ R	2.187	0.486	0.609	2.175	0.504	0.593	2.168	0.483	0.510
R	2.074			2.028			2.060		
Mn1	1.796			1.766			1.785		
Mn2	2.107			2.15			2.070		
D12i ₂ R	2.178	0.447	0	2.157	0.454	0	2.160	0.453	0
R	2.195			2.178			2.178		
Mn1	1.860			1.843			1.845		
Mn2	1.890			1.872			1.870		
D12i ₃ R	2.179	0.427	0	2.157	0.454	0	2.163	0.446	0
R	2.212			2.200			2.187		
Mn1	1.836			1.848			1.836		
Mn2	1.836			1.848			1.836		
D6h ₁ R	2.374	0.452	0.782	2.301	0.460	0.720	2.318	0.467	0.888
R	2.374			2.301			2.318		
Mn2	1.666			1.712			1.698		
Mn2	1.666			1.712			1.698		
D6h ₂ R	2.200	0.454	0	2.175	0.448	0	2.184	0.458	0
R	2.200			2.175			2.184		
Mn2	1.836			1.842			1.852		
Mn2	1.836			1.842			1.852		

0.65 GPa, the superstructural peaks disappear, and diffuse antiferromagnetic scattering is observed in the spectra. When the pressure increases to 6 GPa, diffraction patterns measured in the paramagnetic region show a splitting of the peak (002), which can be interpreted as disintegration into two phases, characterized by volume per formula unit 64.3 and 62.7 Å³ and the ratios of the hexagonal axes are 1.67 and 1.64, respectively. The parameters of the crystalline structure of the high pressure phase approach the values characteristic of most known hexagonal hydrides

RMn_2D_3 , characterized by highly disordered hydrogen sublattice.

4. Results and discussion

The structural and magnetic properties of hexagonal hydrides $RMn_2D_{3-\delta}$ differ greatly from the properties of their cubic analogues. In hexagonal hydrides $RMn_2D_{3-\delta}$ near room temperature, the ordered state is formed in

Table 5. Interatomic distances between R and Mn atoms (d_{R-Mn}), in pairs of Mn atoms doped with hydrogen atoms (d_{Mn-Mn}^D), and free from it (d_{Mn-Mn}), measured near room temperature.

Interatomic distances	Y Mn_2D_3	Tb $Mn_2D_{2.86}$	Dy $Mn_2D_{2.89}$
d_{R-Mn1} , Å	3.357(2)	3.326(1)	3.329(2)
d_{R-Mn2} , Å	3.369(2)	3.334(1)	3.343(2)
d_{R-Mn2} , Å	3.381(2)	3.383(1)	3.358(2)
$d_{Mn1-Mn2}^D$, Å	2.933(2)	2.878(1)	2.887(2)
$d_{Mn2-Mn2}^D$, Å	2.966(2)	2.848(1)	2.888(2)
$d_{Mn2-Mn2}$, Å	2.755(2)	2.818(1)	2.785(2)

the hydrogen sublattice with decrease in the symmetry of the crystalline lattice to $P6_3/m$, in which the equivalent interstitial sites R_2Mn_2 are divided into six independent groups, of which only two are occupied by hydrogen atoms. In cubic analogues the hydrogen is equally distributed over all interstitial sites R_2Mn_2 . Unlike cubic hydrides, where tetragonal interstitial sites have approximately the same size, in hexagonal compounds $RMn_2D_{3-\delta}$ interstitial sites R_2Mn_2 occupied by hydrogen turn out to be distorted, their radii exceed the radii of the remaining interstitial sites (Table 4) and, as a consequence, the „hydrogen volume“ exceeds the values characteristic of hydrides of cubic compounds.

In hexagonal hydrides of stable Laves phases RMn_2D_3 ($R = Er, Tm, Lu$) [7], there are no signs of the hydrogen superstructure formation: hydrogen is disordered along the interstitial sites R_2Mn_2 , and the values of the „hydrogen volume“ and the ratio of the hexagonal axes c/a do not exceed the values characteristic of hydrides of intermetallic compounds. Hexagonal and cubic modifications of intermetallic compounds RMn_2 differ in the packing of atomic layers along the axis c . We can expect that the metastable phase C14, obtained at high pressures, contains a certain number of stacking faults that are not detected by standard powder diffraction methods. We assume that the hydrogen introduction into a metastable metal matrix reveals a hidden instability of the crystalline structure with respect to stacking faults, and the formation of hydrogen superstructure, accompanied by decrease in symmetry, can serve as a kind of marker of errors in the alternation of atomic layers along the axis c .

Hydrogen ordering significantly changes the magnetic properties of hexagonal hydrides $RMn_2D_{3-\delta}$. Due to the deformation of interstitial sites occupied with hydrogen, the distances between magnetic ions inside atomic layers and between them turn out to be nonequivalent (Table 5). The interatomic distances scattering leads to the coexistence of types of exchange interactions of different magnitude and, possibly, sign at the point of magnetic transition, as a

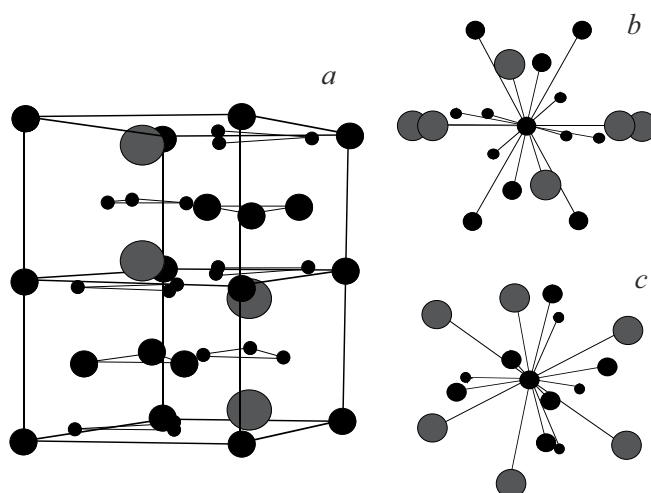


Figure 4. Schematic representation of the crystal structure of the hydrides $RMn_2D_{3-\delta}$ (a). Coordination environment of Mn1 (b) and Mn2 (c) atoms. R atoms are indicated by large gray circles, Mn atoms — by medium-sized black circles, and D atoms — by small black circles.

consequence, the variety of magnetic properties observed in hydrides $RMn_2H_{3-\delta}$ may be due to their competition.

In addition to the crystal lattice distortion, the ordering of hydrogen atoms changes the local environment of magnetic atoms. It is known that the exchange interaction between localized magnetic moments on Mn atoms is isotropic and negative. However, in papers [3,4,6] it was shown that the presence of hydrogen near a pair of Mn atoms can change the sign of the exchange interaction. The superstructure $P6_3/m$ contains two nonequivalent types of positions Mn1 and Mn2, which have 6 and 4 hydrogen atoms in the immediate environment, respectively (Figure 4). Hydrogen atoms are distributed over two types of tetrahedral interstitial sites D1 and D2. D1 atoms are located near each pair of Mn1–Mn2 atoms, and D2 atoms are located in kagome planes formed by Mn2 atoms. Of two neighboring interstitial sites in the Mn2 plane only one can be occupied by hydrogen, since the distance between neighboring interstitial sites is less than the blocking radius. Thus, it turns out that half of the Mn triangles in the kagome plane are surrounded by hydrogen, while the other half are not. Using the approach proposed in papers [3,4,6], we could expect that an antiferromagnetic order will form in the layers of Mn2 atoms, the interaction between the atomic layers Mn1 and Mn2, in its turn, will be ferromagnetic. However, the hydrogen distribution in Mn2 planes, characteristic of the $RMn_2D_{3-\delta}$ superstructure, prevents the establishment of magnetic order in the three-dimensional lattice.

Figure 5, a shows a schematic representation of the magnetic structure of YMn_2D_3 , the parameters of which are given in Table 2. Antiferromagnetic order with wave vector $[1/3\ 1/3\ 0]$ is formed in layers of Mn2 atoms (Figure 5, b), which consist of triangles, the sides of which correspond to the largest and the smallest interatomic distances

d_{Mn-Mn} (Table 5). Large triangles surrounded by hydrogen atoms are ordered ferromagnetically (exchange integral $J_{Mn2-Mn2}^D > 0$), on the contrary, small Mn2 triangles free of hydrogen are ordered antiferromagnetically ($J_{Mn2-Mn2} < 0$) (Figure 5, *b*). The triangular lattice is frustrated with respect to antiferromagnetic interactions, therefore, non-degenerate magnetic state cannot be realized in triangles free of hydrogen; however, 120° -spin configuration realized in magnetic structures with wave vector $[1/3\ 1/3\ 0]$ turns out to be a good compromise for removing degeneracy in the magnetic subsystem. Triangles with 120° -spin configuration are elements of a chain of tetrahedra formed by atoms Mn1 and Mn2 along the axis *c* (Figure 5, *c*). D1 atoms are located near each pair of atoms Mn1–Mn2 forming the faces of the tetrahedron, therefore the exchange interaction between Mn1 and Mn2 atoms is assumed to be ferromagnetic ($J_{Mn1-Mn2}^D > 0$). This configuration of exchange interactions leads to the fact that the resulting exchange field on Mn1 atoms tends to zero, and the planes of Mn1 atoms remain disordered. A similar manifestation of the relationship between chemical and magnetic ordering was discovered in the hydrides $RMn_2D_{4.2}$ ($R = Er, Tm, Lu$) [6], where with similar distribution of hydrogen over D2 positions, short-range order antiferromagnetic correlations were observed.

In hydrides $RMn_2D_{3-\delta}$ with magnetic ions $R = Tb, Dy$, ferrimagnetic order is observed. A schematic representation of the magnetic structure is shown in Figure 6, *a*. The magnetization vectors *R*- and Mn-sublattices are directed

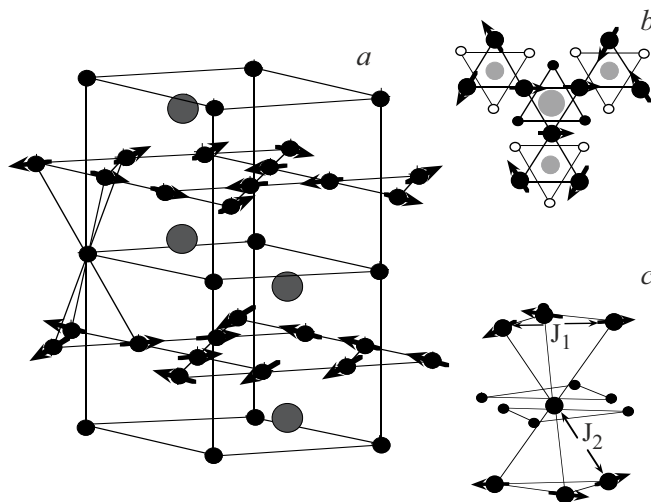


Figure 5. Schematic representation of the magnetic structure of YMn_2D_3 (*a*) and its fragments in the plane containing atoms Mn2 (*b*) and between layers Mn1 and Mn2 (*c*). The fragments show the environment of magnetic ions by atoms D and various types of exchange interactions (J_1 corresponds to $J_{Mn2-Mn2}$, $J_2 - J_{Mn1-Mn2}^D$). Atoms *R* are indicated by large gray circles, Mn atoms — by medium-sized black circles, occupied positions of D atoms — by small black circles, unoccupied positions of D atoms — by small unfilled circles. In the kagome plane gray circles indicate the projections of atoms *R* and Mn1 belonging to neighboring atomic layers.

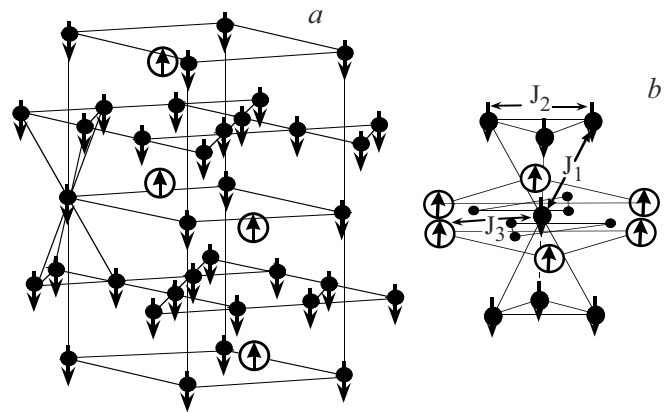


Figure 6. Schematic representation of the magnetic structure of $RMn_2D_{3-\delta}$ ($R = Tb, Dy$) (*a*) and its fragment reflecting the nearest coordination environment of Mn1 atom and various types of exchange interactions (J_1 corresponds to $J_{Mn1-Mn2}^D$, $J_2 - J_{Mn2-Mn2}$, $J_3 - J_{Mn1-R}^D$) (*b*). Atoms *R* are indicated by large unfilled circles, Mn atoms — by medium-sized black circles, D atoms — by small black circles.

towards each other and oriented along the hexagonal axis *c*. Ferromagnetism in the Mn-sublattice was never before observed in the hydrides RMn_2H_x . In cubic analogues the complex noncollinear magnetic structures are realized; however, the ferromagnetic component of the magnetic moment in them is negligibly small [13]. Similar phenomena were discovered in the initial intermetallic compounds RMn_2 ($R = Tb, Dy$) [14,15], in which the distances between Mn atoms lie below the threshold value $d_c = 2.68 \text{ \AA}$, separating the regions of existence of band and localized magnetism in the Mn-sublattice, and ferromagnetic order is a consequence of the magnetic moments ordering on Mn atoms induced by the crystal field of REM ions. This is indicated by the rather low values of T_C and magnetization of the Mn-sublattice ($T_C = 10$ and 40 K , $M_{Mn} = 1.2$ and $0.8 \mu_B$ for $TbMn_2$ and $DyMn_2$, respectively), complex „mixed“ magnetic structures in which only part of the Mn atoms is ordered ferromagnetically, and the rest are ordered antiferromagnetically ($TbMn_2$) or remain non-magnetic ($DyMn_2$), as well as the lack of magnetic ordering in YMn_2 [8].

In hydrides $RMn_2D_{3-\delta}$ interatomic distances d_{Mn-Mn} exceed the threshold value d_c (Table 5), and the magnetic sublattices are ordered simultaneously at $T = 200 \text{ K}$. In papers [3,4,6] it was shown that ordering in *R*-sublattice occurs under the influence of field from Mn ions. The hydrogen superstructure $P6_3/m$ stimulates the formation of ordered magnetic moment in the *R*-sublattice. When D2 positions are occupied with hydrogen, six of the nine Mn2 atoms from the immediate environment of the rare-earth ion turn out to be ferromagnetically ordered, and the exchange field on the rare-earth ions differs from zero. It is possible that in hydrides $RMn_2D_{3-\delta}$ a situation arises when the intersublattice exchange interaction is comparable

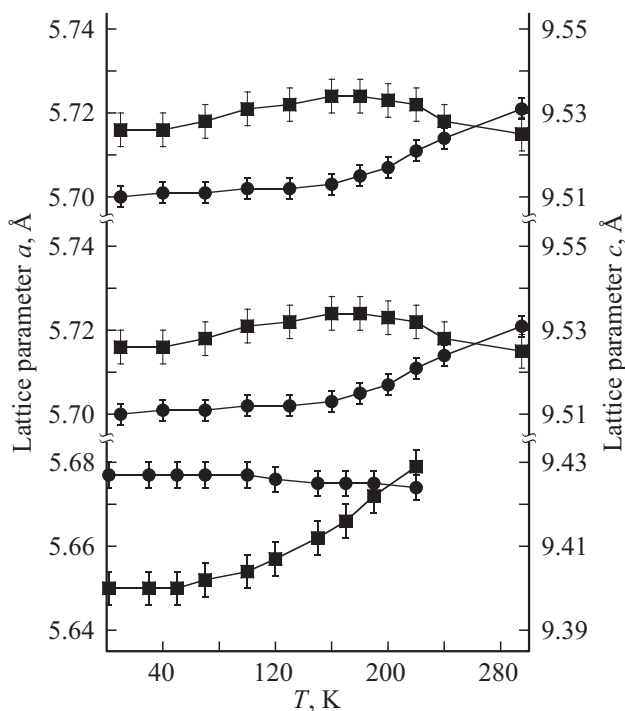


Figure 7. Temperature dependences of the lattice parameters of hydrides $RMn_2D_{3-\delta}$ (from top to bottom YMn_2D_3 , $TbMn_2D_{2.86}$ and $DyMn_2D_{2.89}$). The circles indicate the temperature dependences of the period a , and the squares — of the period c .

in magnitude to the energy of magnetic anisotropy of R -sublattice, and both magnetic sublattices are reoriented in the direction of easy magnetization characteristic of R ions at the magnetic transition point. Similar spin-reorientation transitions were observed in cubic hydrides; in $DyMn_2D_{4.2}$ magnetic moments in both sublattices are oriented along $[111]$ direction and form a phase of the „easy axis“ type, throughout the entire range of existence of magnetic ordering, while in $YMn_2D_{4.2}$ a phase of the „easy plane“ type is observed, in which the magnetization vector of the Mn-sublattice $[\bar{2}11]$ lies in plane perpendicular to the direction $[111]$ [4,17].

The crystal field of magnetic ions R can indirectly modify the configuration of exchange interactions in the Mn-sublattice through change in the orientation of the magnetizations of the Mn and R -sublattices and, as a consequence, magnetostrictive deformation [18]. It is assumed that, due to magnetostriction and/or thermal expansion the lattice parameters take on certain critical values, at which the exchange interaction integral changes sign. Figure 7 shows the temperature dependences of the lattice parameters of the hydrides YMn_2D_3 , $TbMn_2D_{2.86}$ and $DyMn_2D_{2.89}$, differences are noted in the behavior of the curves at the point of magnetic transition in YMn_2D_3 and $DyMn_2D_{2.89}$. In $DyMn_2D_{2.89}$ there are no anomalies in the temperature expansion curves at the magnetic transition point, in the diffraction spectra of $DyMn_2D_{2.89}$, antiferromagnetic correlations are least clearly expressed;

apparently, in this compound the interaction between the layers of Mn1 and Mn2 atoms dominates, resulting in the formation of ferromagnetic order in the Mn-sublattice.

On the contrary, the presence of pronounced diffuse peaks, characterized by the wave vector $[1/3\ 1/3\ 0]$, in the diffraction spectra and the presence of features in the temperature dependences of the lattice periods at the magnetic transition point in $TbMn_2D_{2.86}$ indicate strong competition between the elastic (magnetostrictive) and exchange contributions to the energy. Probably, in $TbMn_2D_{2.86}$ the intermediate situation is realized when the magnitudes of exchange interactions inside the magnetic layers of Mn atoms and between them are comparable, and the transition from ferromagnetic to antiferromagnetic state is easy to initiate by changing the balance of exchange interactions, by changing interatomic distances when high pressures are applied. This assumption is confirmed by the results of experiments at high pressures, in which „crystallization“ of antiferromagnetic order was observed as the external pressure increased.

5. Conclusion

As conclusion, we note that changes in the coordination environment of magnetic ions that arise during the formation of the hydrogen superstructure $RMn_2D_{3-\delta}$ cause a number of unusual magnetic effects never seen before in hydrides RMn_2H_x . Distortions of the crystal lattice, namely the scattering of interatomic distances in the Mn-sublattice, and the unequal surrounding of magnetic ions by hydrogen atoms lead to the fact that at the point of magnetic transition, types of exchange interactions of different magnitude and sign coexist. Antiferromagnetic order in YMn_2D_3 , coexistence of ferrimagnetic and antiferromagnetic correlations of order in $RMn_2D_{3-\delta}$ ($R = Tb, Dy$) and the pressure-induced transition from the ferrimagnetic to the antiferromagnetic state in $TbMn_2D_{2.86}$ is explained by the competition of exchange interactions between nearby Mn atoms, the magnitude and sign of which are determined by the topology of the crystal lattice.

Conflict of interest

The authors declare that they have no conflict of interest.

References

- [1] H. Nakamura, R. Suefuji, S. Sugimoto, M. Okada, M. Homma. *J. Appl. Phys.* **76**, 6828 (1994).
- [2] A. Fujita, S. Fujieda, Y. Hasegawa, K. Fukamichi. *Phys. Rev. B* **67**, 104416 (2003).
- [3] I.N. Goncharenko, I. Mirebeau, A.V. Irodova, E. Suard. *Phys. Rev. B* **56**, 2580 (1997).
- [4] I.N. Goncharenko, I. Mirebeau, A.V. Irodova, E. Suard. *Phys. Rev. B* **59**, 9324 (1999).
- [5] L.A. Stashkova, V.S. Gaviko, N.V. Mushnikov, P.B. Terentyev. *FMM* **114**, 1068 (2013). (in Russian).

- [6] O.L. Makarova, I.N. Goncharenko, A.V. Irodova, I. Mirebeau, E. Suard. *Phys. Rev. B* **66**, 104423 (2002).
- [7] O.L. Makarova, I.N. Goncharenko, F. Bourée. *Phys. Rev. B* **67**, 134418 (2003).
- [8] K. Inoue, Y. Nakamura, A.V. Tsvyashchenko, L.N. Fomicheva. *J. Phys. Soc. Jpn.* **64**, 2175 (1997).
- [9] A.V. Tsvyashchenko, A.I. Velichkov, A.V. Salamatin, L.N. Fomicheva, D.A. Salamatin, G.K. Ryasny, A.V. Nikolaev, M. Budzynski, R.A. Sadykov, A.V. Spasskiy. *J. Alloys Compd.* **552**, 190 (2013).
- [10] I.N. Goncharenko. *High Press. Res.* **24**, 193 (2004).
- [11] J. Rodriguez-Carvajal. *Physica B* **192**, 55 (1993).
- [12] A.C. Switendick. *Z. Phys. Chem.* **117**, S89 (1979).
- [13] H. Figiel, J. Przewoznik, V. Paul-Boncour, A. Lindbaum, E. Gratz, M. Latroche, M. Escorn, A. Percheron-Guegan, P. Mietniowski. *J. Alloys Compd.* **274**, 29 (1998).
- [14] K. Inoue, Y. Nakamura, Y. Yamaguchi, M. Ohashi, K. Ohoyama, S. Funahashi, A.V. Tsvyashchenko, L. Fomicheva. *J. Phys. Soc. Jpn.* **64**, 4489 (1995).
- [15] K. Inoue, Y. Nakamura, Y. Yamaguchi, K. Ohoyama, M. Ohashi, A.V. Tsvyashchenko, L. Fomicheva. *J. Phys. Soc. Jpn.* **67**, 4306 (1998).
- [16] M. Shiga. *Physica B* **149**, 293 (1988).
- [17] O.L. Makarova, I.N. Goncharenko, I. Mirebeau. *Phys. Rev. B* **59**, 11826 (1999).
- [18] C. Kittel. *Phys. Rev.* **120**, 335 (1960).

Translated by I.Mazurov